3D Dynamic T1 Mapping of the Myocardium Using a Time-Varying Subspace

Anthony G. Christodoulou[1] and Zhi-Pei Liang[1]

[1]*Beckman Institute and Department of Electrical and Computer Engineering, University of Illinois at Urbana-Champaign, Urbana, IL, United States*

INTRODUCTION

T_1 mapping of the myocardium shows great promise for quantitative characterization of myocardial tissue. For example, quantification of myocardial T_1 both before and after contrast agent administration allows measurement of the extracellular volume fraction, allowing identification of global abnormalities where qualitative imaging cannot. Unfortunately, parameter mapping increases the already-challenging data acquisition requirements of cardiovascular imaging, requiring multiple contrast weightings in order to extract parameter values. The partial separability (PS) model [1] has previously been shown as effective for reducing the data acquisition requirements of static parameter mapping; here we extend the PS model to accelerate variable-flip-angle dynamic 3D T_1 mapping using a time-varying subspace.

METHODS

We model the image function as partially separable in space, time, and flip angle [1]:

$$\rho(\mathbf{r},t,\alpha)=\sum_{\ell=1}^{L}\sum_{m=1}^{M}\sum_{n=1}^{N}c_{\ell mn}u_\ell(\mathbf{r})v_m(t)w_n(\alpha) \qquad (1)$$

This decomposition can be viewed as representing ρ as a low-rank tensor, or more precisely, as a rank-(L,M,N) tensor [2]. This model motivates a data acquisition strategy wherein we collect navigator data by densely sampling $(\mathbf{k},t,\alpha)$-space over limited regions of $(\mathbf{k},t)$-space and $(\mathbf{k},\alpha)$-space, as well as imaging data by sparsely sampling the remainder of $(\mathbf{k},t,\alpha)$-space.

For the basic PS model, it is common to determine the subspace structure from the singular value decomposition (SVD) of a Casorati matrix containing navigator data. For this higher-order PS model, the navigator data from the densely sampled $(\mathbf{k},t)$-space and $(\mathbf{k},\alpha)$-space locations enable the definition of two "Casorati tensors". We collapse the Casorati tensors along different dimensions (either the t or α dimensions), forming two Casorati matrices: $\mathbf{C}_1$, the jth column of which contains the samples $d\left(\{\mathbf{k}_p\}_{p=1}^{P},t_j,\{\alpha_p\}_{p=1}^{P}\right)$, where $\{(\boldsymbol{k}_p,\alpha_p)\}_{p=1}^{P}$ is the set of $(\mathbf{k},\alpha)$-space locations that contain data from all time points; and $\mathbf{C}_2$, the jth column of which contains the samples $d\left(\{\mathbf{k}_q\}_{q=1}^{Q},\{t_q\}_{q=1}^{Q},\alpha_j\right)$, where $\{(\boldsymbol{k}_q,t_q)\}_{q=1}^{Q}$ is the set of $(\mathbf{k},t)$-space locations that contain data from all flip angles. The M most significant right singular vectors of $\mathbf{C}_1$ yield basis functions $\{v_m(t)\}_{m=1}^{M}$; the N most significant right singular vectors of $\mathbf{C}_2$ yield basis functions $\{w_n(\alpha)\}_{n=1}^{N}$.

It is simple to show that the decomposition in Eq. 1 can be expressed as: $\rho(\mathbf{r},t,\alpha)=\sum_{\ell=1}^{L}u_\ell(\mathbf{r})\psi_\ell(t,\alpha)$, where $\psi_\ell(t,\alpha)=\sum_{m=1}^{M}\sum_{n=1}^{N}c_{\ell mn}v_m(t)w_n(\alpha)$. Without knowledge of the c, we can define $\hat{L}=MN$ functions $\hat{\psi}_\ell(t,\alpha)=\hat{\psi}_{m,n}(t,\alpha)=v_m(t)w_n(\alpha)$ (where ℓ indexes the Cartesian set of m,n pairings). Noting that $\{\hat{\psi}_\ell(t,\alpha)\}_{\ell=1}^{\hat{L}}$ defines a tensor-product subspace that contains the subspace spanned by $\{\psi_\ell(t,\alpha)\}_{\ell=1}^{L}$, we can use $\rho(\mathbf{r},t,\alpha)=\sum_{\ell=1}^{\hat{L}}u_\ell(\mathbf{r})\hat{\psi}_\ell(t,\alpha)$ for image reconstruction. More specifically, we solve the following optimization problem to recover $\{u_\ell(\mathbf{r})\}_{\ell=1}^{\hat{L}}$ from the imaging data sparsely sampling $(\mathbf{k},t,\alpha)$-space:

$$\arg\min_{\{u_\ell(\mathbf{r})\}_{\ell=1}^{\hat{L}}}\left\|\mathbf{d}-\Omega\left\{\sum_{\ell=1}^{\hat{L}}\mathcal{F}_{\mathbf{r}}\{u_\ell(\mathbf{r})\}\hat{\psi}_\ell(t,\alpha)\right\}\right\|_2^2+R\left(\{u_\ell(\mathbf{r})\}_{\ell=1}^{\hat{L}}\right),$$

where $\mathbf{d}$ is the vector of measured data, Ω is the sparse sampling operator, and R is a regularization function, which can be chosen to be a weighted L2 penalty function or sparsity-promoting L1 penalty.

RESULTS AND DISCUSSION

In order to create a gold standard with biologically relevant T_1 variation, we imaged male Brown Norway (BN) rats with 45 min transient left circumflex (LCx) coronary artery occlusion followed by re-perfusion. Data were collected on a Bruker Avance AV1 4.7 T / 40 cm scanner with a 4-channel phased array coil. A 0.2 mmol/kg bolus of gadolinium contrast agent was administered, and four real-time 3D FLASH scans using α = 3°, 19°, 22°, and 28° were collected during the steady-state of contrast and reconstructed as one extended time sequence using the image model described in [3]. Images were collected with T_R/T_E = 10/2.5 ms, FOV = 40 mm × 40 mm × 24 mm, matrix size = 96 × 96 × 24, and spatial resolution = 0.42 mm × 0.42 mm × 1.0 mm.

We then performed T_1 fitting for one respiratory cycle (89 frames) and generated images for 10 flip angles (2°, 5°, 10°, 15°, 20°, 25°, 30°, 35°, 40°, and 45°). We compared two navigator sampling strategies: 1) dense sampling of $(\boldsymbol{k},t,\alpha)$-space over an $8\times96\times8$ $\mathbf{k}$-space region; and 2) dense sampling of $(\boldsymbol{k},t,\alpha)$-space over a $16\times96\times16$ $\mathbf{k}$-space region for only three time points and two flip angles (2°, 45°). The two strategies collect the same amount of navigator data. We randomly undersampled the remainder of $(\mathbf{k},t,\alpha)$-space by a factor of 16.5 for a total undersampling factor of 11.5.

Figure 1 shows gold standard and accelerated R_1 maps for one slice and time point of the image sequence. The regularization function R was chosen to impose anatomical edge constraints [4] generated from a composite image as in [5]. Elevated R_1 values are visible in the anterior and lateral myocardium, indicating ischemic reperfusion injury. Both accelerated image sequences accurately represent R_1.

CONCLUSION

This paper presents a novel method for accelerated 3D dynamic T_1 mapping of the myocardium, exploiting the tensor structure of the underlying multivariate image function of space, time, and flip angle. The method will prove useful for quantitative characterization of myocardial tissue.

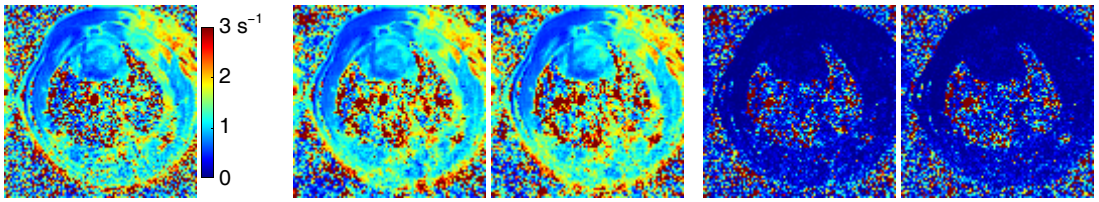

(a) (b) (c) (d) (e)

Fig. 1: Slices of R_1 maps from one time point of (a) the gold standard and 11.5x-accelerated images using (a) navigator strategy 1, and (b) navigator strategy 2. (d) and (e) are error maps for (b) and (c), respectively.

REFERENCES

[1] Z.-P. Liang, *IEEE-ISBI* 2007, pp. 988-91. [2] T. G. Kolda and B. W. Bader, *SIAM J Matrix Anal Appl* 2009, pp. 455-500.
[3] A. G. Christodoulou, *et al.*, *IEEE-TBME* 2013, pp. 3083-92. [4] J. P. Haldar, *et al.*, *MRM* 2008, pp. 810-8. [5] A. G. Christodoulou, *et al.*, *IEEE-EMBC* 2010, pp. 871-4.